THE JOURNAL OF PHYSICAL CHEMISTRY C

Article

pubs.acs.org/JPCC

Layer-Resolved Evolution of Organic Thin Films Monitored by Photoelectron Emission Microscopy and Optical Reflectance Spectroscopy

Ebrahim Ghanbari,* Thorsten Wagner,* and Peter Zeppenfeld*

Institute of Experimental Physics, Johannes Kepler University, Altenberger Str. 69, 4040 Linz, Austria

Supporting Information

ABSTRACT: Photoelectron emission microscopy (PEEM) and differential (optical) reflectance spectroscopy (DRS) have proven independently to be versatile analytical tools for monitoring the evolution of organic thin films during growth. In this paper, we present the first experiment in which both techniques have been applied simultaneously and synchronously. We illustrate how the combined PEEM and DRS results can be correlated to obtain an extended perspective on the electronic and optical properties of a molecular film dependent on the film thickness and morphology. As an example, we studied the deposition of the organic molecule α-sexithiophene on Ag(111) in the thickness range from submonolayers up to several monolayers.

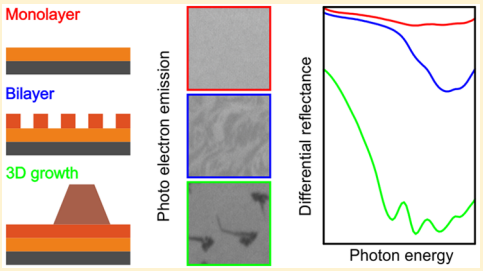

INTRODUCTION

The optical and electronic properties of π-conjugated organic materials have been the subject of intense research because of their considerable fundamental and technological importance.[1−3] These properties are defined not only by the chemical structure of the constituting molecules but also by their intermolecular coupling. For instance, in the solid state, it is expected that these properties are affected by the molecular packing. In addition, the orientation of π-stacked molecules with respect to the electrodes is of great relevance for the performance of devices, such as organic field effect transistors (OFETs)[4,5] and organic light-emitting diodes (OLEDs).[4,6,7] Therefore, controlling the molecular orientation and stacking is crucial.

In-situ and/or real-time information during growth of organic thin films has been obtained with a variety of analytical techniques, such as reflection high-energy electron diffraction (RHEED)[8] or low-energy electron diffraction (LEED),[9−12] X-ray reflectivity (XRR),[13] X-ray diffraction (XRD),[14] or X-ray standing waves (XSW),[15,16] photoelectron spectroscopy (UPS, XPS),[17−19] or photoelectron emission microscopy (PEEM).[20−25] In addition, optical methods such as differential reflectance spectroscopy (DRS)[1,3,26,27] and reflectance difference spectroscopy (RDS)[28,29] are perfectly suited for in situ and real-time monitoring of organic thin film growth.

In this work, we report on the coverage dependence of the excitonic states[30] in an organic thin film deposited on a metal surface. In particular, we show how photoelectron emission microscopy and differential reflectance spectroscopy can be acquired *simultaneously* to monitor the growth of α-sexithiophene on a Ag(111) surface in real-time.

α-sexithiophene (α-6T) is a well-known organic dye pigment which constitutes a model system to study the photophysical properties of π-conjugated molecules. The strong involvement of Franck−Condon and Herzberg−Teller types of vibronic coupling makes this member of the oligothiophene family a prototype for the studies of crystals and thin films.[31−34]

Because the first monolayer acts as a template for further growth, it has a strong influence on the structure and, hence, on the electronic and optical properties of the entire organic film. Therefore, it is of particular importance to characterize and control the interface between the organic layer and the substrate.[21,28,35] Here, we consider metal substrates because they may exhibit a strong interaction with the organic molecules and the lateral ordering, at least within the monolayer, will be governed by the subtle interplay between substrate−adsorbate and adsorbate−adsorbate interactions.

While we have previously studied the deposition of α-6T on Ag(110) surfaces[21,24,36] using PEEM and STM, we have selected a Ag(111) single crystal as substrate for this study to avoid any effects of optical anisotropy in the DRS. Silver substrates are also particularly well suited for PEEM studies in the lab, because the light of the standard Hg lamp provides photons with an energy that is high enough to excite electrons across the work function barrier at the silver surface.

It has been reported that α-6T adsorbs on Ag(110) and Ag(111) surfaces such that its molecular plane is almost parallel to the substrate surface irrespective of film thickness.[8] The α-6T molecules are azimuthally aligned on the Ag(111) surface, exhibiting a 6-fold symmetry in the surface plane. In this configuration, the long molecular axis of the α-6T molecules is oriented along one of the $\langle 1\bar{1}0\rangle$ directions.[8] The structure found in the thin film phase is quite different from that of bulk single-crystals, in which the α-6T molecules stack in a

Received: August 19, 2015
Revised: September 29, 2015
Published: October 1, 2015

DOI: 10.1021/acs.jpcc.5b08083
J. Phys. Chem. C 2015, 119, 24174−24181

herringbone packing with the molecular planes of adjacent molecules tilted by 66° with respect to each other.

EXPERIMENTAL SECTION

The experiments were performed in a ultrahigh vacuum chamber with a base pressure of 3×10^{-10} mbar. The Ag(111) single crystal was cleaned by repeated cycles of Ar^+ ion sputtering (900 V, 3.8 $\mu A/cm^2$) and annealing at 660 K. The commercially available α-6T was purified by gradient sublimation. The organic films were prepared by thermal evaporation of the α-6T while PEEM and DRS were triggered for simultaneous and synchronous data acquisition; see Figure 1 for details of the experimental setup. To avoid any influence

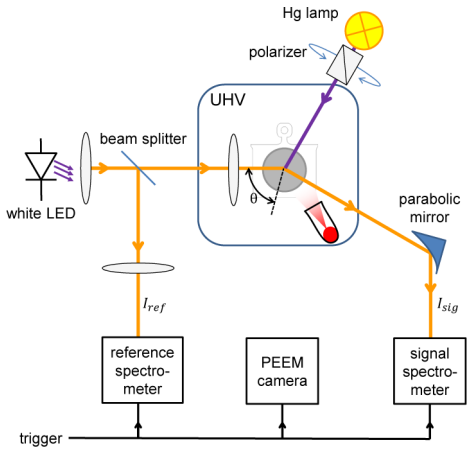

Figure 1. Schematic of the setup combining photoelectron emission microscopy (PEEM) and differential reflectance spectroscopy (DRS). PEEM images and DRS spectra can be acquired *synchronously* from the same sample. The surface normal of the sample is oriented parallel to the electron column of the PEEM instrument. Both light beams, that of the white LED used for DRS and that of the Hg lamp used for the PEEM, exhibit a (polar) angle of incidence of $\theta = (65 \pm 3)°$ with respect to the surface normal, but are rotated azimuthally by 120° around the surface normal (PEEM column).

of the deposition rate on the crystallographic phases of the α-6T film,[13] the quartz-crucible containing the α-6T was held at a fixed temperature to ensure a constant deposition rate.

The PEEM is operated with a high-pressure mercury arc discharge (Hg) lamp which generates photons with energies up to 4.9 eV. This excitation energy is sufficient to emit enough electrons for imaging. The light can be linearly polarized using a rotatable calcite Glan−Thomson prism. For the experiments in this paper, the incident light of the Hg lamp was p-polarized, resulting in a maximum electron yield.[24] The interplay between photoelectron emission and the (linear) polarization state of the exciting photons can be used to distinguish different orientations of organic molecules in nanostructures, as we demonstrated recently in ref 37.

The DRS is operated in a "two-beam configuration"[38] in which a fraction of the incident light is detected simultaneously with the reflected beam to correct for intensity fluctuations of the light source. Because of its spectral composition, the Hg arc discharge lamp is not suitable for high-resolution DRS measurements in the visible range. Therefore, an additional white LED was mounted in front of another viewport under an angle of $\theta \approx 65°$ with respect to the surface normal. A beam splitter is used to couple out a part of the incident beam which is then detected by the reference spectrometer. The other part of the beam is reflected from the sample surface and focused by an off-axis parabolic mirror into the signal spectrometer. The signal and reference spectrometers are of the same type (Ocean Optics STS-VIS, equipped with diode arrays spanning a photon energy range from 1.5 to 3.6 eV). The synchronously measured spectra $I_{sig}(E,t)$ and $I_{ref}(E,t)$ from both detectors are used to obtain a normalized intensity spectrum $I_n(E,t)$ that is strictly proportional to the reflectance $R(E,t)$ at a given photon energy E and time t:

$$I_n(E,t) = \frac{I_{sig}(E,t) - I_{sig,dark}(E,t)}{I_{ref}(E,t) - I_{ref,dark}(E,t)} \propto R(E,t) \quad (1)$$

The DRS spectrum, i.e., the normalized difference in reflectivity,[3] is obtained from the normalized intensities, I_n, in eq 1 via

$$\mathrm{DRS} \equiv \frac{\Delta R}{R_0} = \frac{R(E,t) - R(E,0)}{R(E,0)} = \frac{I_n(E,t) - I_n(E,0)}{I_n(E,0)} \quad (2)$$

Here $R_0 = R(E,0)$ and $I_n(E,0)$ denote the reflectance and intensity spectra of the pristine surface, respectively, recorded just before the shutter in front of the evaporator is opened to start the growth experiment ($t = 0$). After the shutter is opened, DRS spectra are recorded in (regular) time steps $t_j = j\Delta t$. The sampling time, Δt, typically amounts to a few seconds, presenting a trade-off between temporal resolution and signal-to-noise ratio. In the end, a two-dimensional (2D) set of data-points, $\mathrm{DRS}(E_i,t_j)$, is obtained, which describes the evolution of the differential reflectance spectra with deposition time. If the deposition rate is constant, t is proportional to the exposure. If, in addition, the sticking coefficient is also constant, t is proportional to the total adsorbed amount of the organic molecules, i.e., the coverage, Θ, or the (nominal) film thickness, d. The whole data set can be visualized as a 2D image by mapping the DRS signal to a gray scale or false-color scale at pixels (i,j) representing the discrete values $\{E_i\}$ and $\{t_j\}$, respectively (see, for instance, Figure 5a). Alternatively, the data can be represented as a series of 1D cuts along the energy or time axes, yielding a time sequence of *spectra* (as in the case of Figure 4) or a number of *transients* at a single photon energy or a specified spectral interval (as shown in Figure 2b).

The gradual changes in the spectral line shape are often better discernible if instead of $\Delta R/R_0$ the incremental changes of the DRS signal between two subsequent time steps are plotted. To this end we define the "differential DRS" spectra, termed DDRS, as the normalized difference between subsequent reflectance measurements:

$$\mathrm{DDRS} \equiv \frac{\Delta R}{\bar{R}} = 2\frac{R(E,t_{j+1}) - R(E,t_j)}{R(E,t_{j+1}) + R(E,t_j)} \quad (3)$$

In contrast to eq 2, the reference to the pristine substrate R_0 is replaced by the reflectance of an "effective substrate" which also includes the organic film grown during the previous deposition steps. The DDRS spectrum thus describes the *differential* changes of the reflectance originating from the very thin slice of the film deposited only during the time interval $[t_j,t_{j+1}]$. Note that the DDRS spectrum as defined in eq 3 is not just the difference between subsequent DRS spectra, which would be $\Delta\mathrm{DRS} = (R(E,t_{j+1}) - R(E,t_{j+1}))/R_0$. In fact, ΔDRS still takes the pristine surface as reference. The difference between DDRS and ΔDRS vanishes if $\bar{R} \approx R_0$, i.e., if the overall changes in

DOI: 10.1021/acs.jpcc.5b08083
J. Phys. Chem. C 2015, 119, 24174−24181

reflectance are small, namely, for ultrathin films consisting of only a couple of molecular layers.

RESULTS AND DISCUSSION

Growth Mode and Morphology of α-6T on Ag(111).

Figure 2 shows a PEEM transient of the local electron yield (LEY) for p-polarized light (Figure 2a) together with the DRS signal $\Delta R/R_0$ at a photon energy of 2.3 eV (Figure 2b) recorded simultaneously during the deposition of α-6T on a clean Ag(111) surface held at 331 K. The PEEM transient shown in Figure 2a was obtained by processing each of more than 1000 PEEM images recorded each 1.2 s during the growth experiment. Selected PEEM images are depicted in Figure 3. The solid cyan line in Figure 2a represents the mean value of the electron yield, averaged over the entire field of view (~145 μm) of each image. A gray scale representation of the histograms, which were calculated for the intensity distribution of each PEEM image, is found underneath the cyan line. Darker shades of gray indicate a higher probability of finding a particular LEY value at time t. Therefore, the blackness and width of the gray band underneath the cyan line is a measure of the spatial variation of the photoemission yield at a given time t.

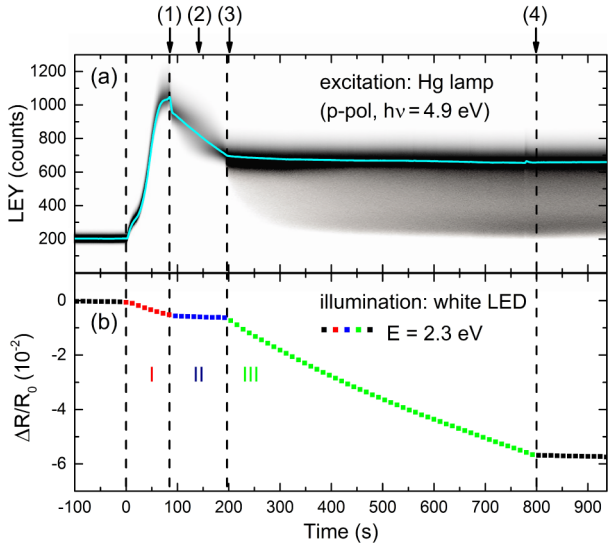

Figure 2. (a) Transient of the PEEM intensity (LEY) recorded during the deposition of α-6T on a Ag(111) surface held at 331 K. The solid cyan line corresponds to the intensity averaged of the entire field of view. The gray area in the background is a gray scale representation of the intensity distribution of each individual image. (b) Transient of the differential reflectance (DRS, $\Delta R/R_0$) at a photon energy E = 2.3 eV. The PEEM and DRS transients were acquired simultaneously and synchronously. α-6T was deposited at a constant rate between t = 0 (shutter opened) and t = 800 s (shutter closed). Vertical dashed lines delimit the three distinct growth stages I, II, and III. Labels 1−4 at the top refer to the PEEM-images depicted in Figure 3.

As can be seen from Figure 2, there is a clear correlation between the PEEM and the DRS transients. In particular, the characteristic changes in the line shape of the PEEM transient and the concomitant kinks in the slope of the DRS transient at t_1 = (85 ± 3) s and t_2 = (197 ± 5) s, respectively, suggest that the growth can be subdivided into three distinct stages, labeled I, II, and III.

(I) $0 < t < t_1$: After the shutter is opened at t = 0, the average PEEM intensity (LEY) increases monotonously up to t_1 where the PEEM transient reaches its maximum. At any time during this stage of growth the PEEM intensity is rather uniform and homogeneously distributed across the entire field of view of the PEEM, as exemplified by image 1 in Figure 3. At the same time, the DRS transient for E = 2.3 eV decreases in an almost linear fashion.

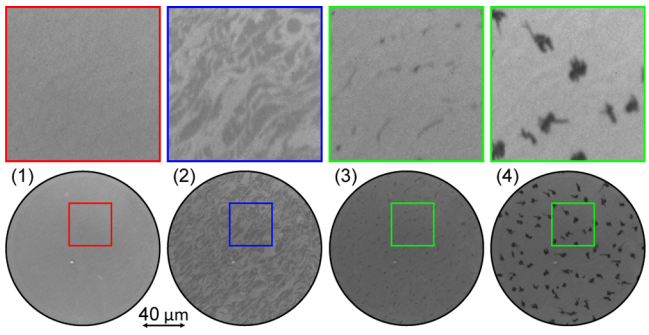

Figure 3. Selected PEEM images recorded during the deposition of α-6T on a Ag(111) surface held at 331 K (Figure 2). The images were taken at times 1−4 marked in Figure 2: (1) maximum intensity of the PEEM transient, corresponding to the completion of the first α-6T monolayer; (2) half way during the formation of the second monolayer; (3) onset of 3D growth after completion of the second monolayer; and (4) thick film (nominal coverage ~8 ML) showing α-6T crystallites on top of the 2 ML thick wetting layer. The images of the lower row correspond to a field of view of 145 μm. The images in the top row show an enlarged view of the 40 × 40 μm^2 area indicated in the images in the bottom row. The color coding of the frames matches the one in Figure 4. The full image sequence is available as Supporting Information.

(II) $t_1 < t < t_2$: The average PEEM intensity decreases monotonically. However, in stark contrast to stage I, the intensity is distributed inhomogeneously across the field of view of the PEEM images, as can be seen in image 2 in Figure 3: bright and dark micrometer-sized patches covering about equal areas can be discerned in this image. With increasing coverage, the relative amount of the dark patches increases continuously at the expense of the brighter ones. At the end of growth stage II, the PEEM intensity is homogeneously distributed again. During growth stage II, the slope of the DRS signal at 2.3 eV (see Figure 2b) is constant and close to zero.

(III) $t > t_2$: Another kink in the PEEM and DRS tansients marks the transition from growth stage II to III. At this point, the PEEM images reveal the onset of nucleation and subsequent growth of 3D islands (see image 3 in Figure 3). α-6T crystallites identified as dark structures appear across the field of view and grow larger upon further deposition of α-6T (image 4 in Figure 3). During stage III, the DRS signal decays monotonically at a gradually decreasing rate. For $t > t_2$, no further abrupt changes are observed in the PEEM transient as well as in the DRS transient until the shutter is closed and both signals do not change any longer.

The PEEM transient in Figure 2 closely resembles the one observed during the growth of α-6T on Ag(110).[24,36] Likewise, the DRS transient shows the same characteristics as the reflectance difference spectroscopy curves recorded during growth of α-6T on Cu(110)(2 × 1)O.[28] As in these previous studies, we associate growth stages I and II with the completion of the first and second monolayer of α-6T, respectively, whereas stage III is related to 3D island nucleation and growth. Consequently, the growth of α-6T on Ag(111) follows the

DOI: 10.1021/acs.jpcc.5b08083
J. Phys. Chem. C 2015, 119, 24174−24181

Stranski−Krastanov mode with a two-monolayer thick wetting layer.

The interpretation of the PEEM transient depicted in Figure 2 follows the same arguments as for α-6T on Ag(110):[24,36,37] The deposition of the first monolayer of α-6T induces a surface dipole. This dipole effectively lowers the work function barrier for the photoemission of electrons excited in the silver substrate[39−41] and leads to the increase of the PEEM intensity during stage I in Figure 2a.

The reported ionization potential of α-6T (ranging from 5.3 to 5.9 eV[39,42,43]) is definitely larger than the energy of the photons provided by the Hg lamp. Therefore, no electrons can be emitted from the α-6T layer under illumination with a Hg lamp such that only electrons from the silver substrate will contribute to the detected photoemission intensity. The adsorbed α-6T will actually reduce the photoemission yield from the substrate due to inelastic scattering of the electrons which have to traverse the organic layer before being emitted into the vacuum. The strong reduction of the work function during the deposition of the first monolayer, however, outweighs the attenuation by the ultrathin monolayer film resulting in a net increase of the PEEM intensity during stage I. Because the work function is not significantly altered upon deposition of α-6T molecules on top of the first monolayer, the average PEEM intensity decreases again during deposition of the second monolayer (stage II) and after nucleation and growth of 3D islands (α-6T crystallites) in stage III. The maximum of the electron yield at $t_1 \approx 85$ s in Figure 2 can thus be assigned to the completion of the first α-6T monolayer (1 ML).

The absence of any spatial inhomogeneity of the PEEM intensity within the field of view during the deposition of the first layer (see image 1 in Figure 3) suggests that the lateral dimensions of the 2D islands are smaller than the resolution limit of the PEEM, which is of the order of 100 nm. We expect that the 2D islands are in dynamic equilibrium with a mobile 2D molecular gas phase, ensuring that the *average* coverage over a typical length scale of 100 nm is spatially rather uniform and increases monotonically with deposition time.

The situation is quite different for the growth of the second layer during stage II. This can be seen in the histograms shown in the background of the PEEM transient in Figure 2a, revealing two intensity levels whose relative proportion changes almost linearly with coverage in the second layer. The origin becomes clear from the associated PEEM images, such as image 2 depicted in Figure 3. The lower intensity level can thus be attributed to large patches where an α-6T bilayer is already established, whereas the brighter regions are still characteristic of the monolayer (which might again be covered by a dilute 2D molecular gas). With increasing coverage the dark patches grow at the expense of the bright areas until a homogeneous α-6T bilayer is formed. In contrast to the monolayer, the condensation and growth of the 2D α-6T islands in the second layer occurs over a length scale $\gtrsim 10$ μm which is readily resolved in the PEEM images. The strong increase of the characteristic length scale could be explained by the increased mobility of the molecules on top of the α-6T monolayer as compared to the pristine Ag(111) surface. Moreover, the formation of the bilayer most likely involves a restructuring of the first layer which might require a larger critical coverage (or critical nucleus size) to locally initiate this transformation of the underlying monolayer. As a result, the bilayer island density will be smaller and the average domain size accordingly larger. Strong evidence for the restructuring of the monolayer upon bilayer formation comes from the fact that the total deposited amount required for completion of the bilayer ($t_2 = 197$ s) is considerably larger than twice the amount needed for completion of the first monolayer ($t_1 = 85$ s). In fact, according to Yoshikawa et al.,[8] the packing density in the monolayer phase of α-6T on Ag(111) is rather small because of the flat-lying geometry of the molecules and the large (commensurate) intermolecular spacing of 6.43 Å along the $\langle 11\bar{2} \rangle$ direction. The ratio $t_2/(2t_1) \approx 1.16$ would imply a significant compression of the first monolayer by $\gtrsim$10%. However, a non-negligible fraction of the deposited molecules during stage II could already reside in the third layer, forming a 2D gas phase in equilibrium with the molecules in the second layer such that the actual compression of the first monolayer may be somewhat smaller. Similar processes are also discussed in refs 22 and 23 for the case of *p*-6P on Cu(110)(2 × 1)O.

At $t_2 = 197$ s, a sharp kink in the PEEM and DRS transients in Figure 2 marks the transition from stage II to III, i.e., the onset of 3D island nucleation. The PEEM image 3 in Figure 3 recorded at this point reveals dark spots indicating the nucleation of α-6T crystallites of significant height. The pronounced drop of the PEEM intensity in these spots is also reflected in the sudden change of the histograms shown in the background of the PEEM transient in Figure 2a which exhibits a tail toward very low intensities. Consequently, the crystallites must have appreciable heights in order to cause this almost complete attenuation of the photoelectron yield from the underlying Ag(111) substrate. On the other hand, the emission from the surrounding wetting layer (consisting of two molecular layers) stays almost constant at the value reached after completion of the bilayer. Upon further deposition of α-6T, the crystallites grow both in size and height (see image 4 in Figure 3). At the end of the growth experiment ($t_e = 800$ s), the amount of the material accumulated in the 3D crystallites is about three times that contained in the wetting layer, whereas only a small fraction of the surface area ($\lesssim$10%) is actually covered by these crystallites. Consequently, the average height of the crystallites amounts to $\gtrsim$20 molecular layers.

As described in the previous paragraphs, the transient of the DRS signal at a photon energy of 2.3 eV is strongly correlated with the morphology observed by PEEM. The photon energy of 2.3 eV was selected in Figure 2b because it shows a strong layer-dependent variation. As evidenced by Figure 2, the slope of the transient of the DRS signal changes abruptly as a function of the α-6T coverage, revealing the same three growth stages as the PEEM transient. The sudden change of the slope of the DRS transient between the first and second growth stage indicates a strict layer-by-layer growth[28] of the first two monolayers: only after the first layer is (almost) completed, the bilayer starts to nucleate on top of it. The onset of the 3D growth is indicated by another change in the slope of the DRS transient (stage III).

Layerwise Evolution of the Optical Properties. More information about the optical properties in correlation with the film morphology (Figure 3) can be obtained by analyzing the spectroscopic evolution of the optical reflectance as a function of the deposition time (α-6T coverage). Figure 4 shows the full spectral range of the DRS signal $\Delta R(E,t)/R_0$ recorded during the same experiment as discussed in Figure 2. The spectra reveal the stepwise evolution of the optical properties with increasing layer thickness. In addition, Figure 5 shows the *incremental* changes between subsequent deposition steps

DOI: 10.1021/acs.jpcc.5b08083
J. Phys. Chem. C 2015, 119, 24174−24181

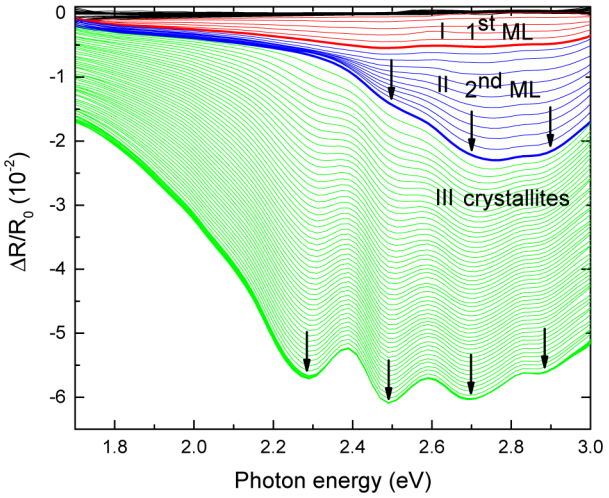

Figure 4. Thickness-dependence of the DRS spectra ($\Delta R/R_0$) recorded during deposition of α-6T on the Ag(111) single crystal. Different colors (red, blue, and green) correspond to the three growth stages (I, II, and III, respectively) as defined in Figure 2. The solid lines mark fundamental electronic transitions and/or their vibronic replica.

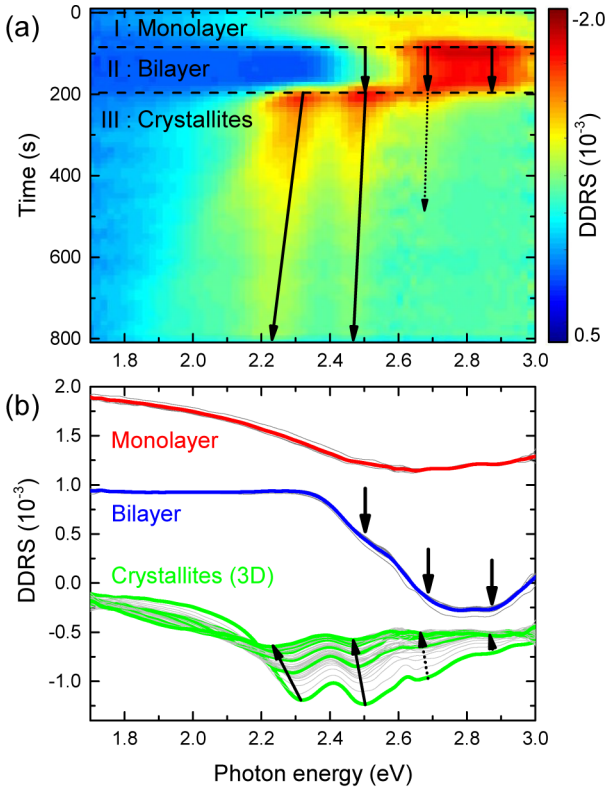

Figure 5. DDRS spectra ($\Delta R/\bar{R}$) based on the same data as Figure 4 but revealing the *incremental* changes of the optical reflectance for α-6T grown on the Ag(111) substrate: (a) false color image and (b) selected individual spectra, characterizing the three stages of growth, namely, the formation of the monolayer, bilayer and 3D crystallites. The red and blue lines represent the average of the spectra characteristic for stages I and II, respectively, whereas the green lines highlight DDRS spectra for equally spaced nominal coverages in the range between 2 and 8 ML. The monolayer and bilayer spectra in panel b were offset by 2×10^{-3} and 1×10^{-3} for clarity.

represented by the *differential* DDRS spectra ($\Delta R/\bar{R}$ as defined in eq 3). In Figure 5 the data are presented as a 2D image in false color representation (Figure 5a) and selected DDRS spectra are shown in (Figure 5b).

During deposition of the first monolayer (stage I), the DRS and DDRS spectra in Figures 4 and 5, respectively, show a weak, broad feature in the spectral range between 2.3 and 2.9 eV. During the formation of the α-6T bilayer (stage II), the DRS and DDRS spectra look completely different compared to those obtained during growth stage I. The spectral weight is shifted to higher energies and the spectra are composed of three overlapping peaks located at about 2.5, 2.7, and 2.9 eV, respectively. Finally, the transition from stage II to stage III is again marked by a sudden change in the spectral line shape. Figure 5 reveals a clear red-shift of the overall spectral weight with prominent peaks at 2.32 and 2.50 eV. Upon further deposition of α-6T, the position of these two peaks shifts continuously to 2.23 and 2.47 eV, respectively. At the same time, their amplitude decreases with increasing film thickness. It should be emphasized that the DRS spectra in Figure 4 recorded at time t display the *total* change of the reflectance after deposition of the entire film grown up to time t, whereas the DDRS spectra in Figure 5 show only the *incremental* change of the reflectivity produced by the molecules deposited within the very last deposition step on the previously grown film. As a result, the DRS spectra recorded during growth stage III still exhibit the features accumulated during the previous growth of the wetting layer, whereas the DDRS spectra in the same growth stage can be assigned, exclusively, to the very last molecules incorporated into the α-6T crystallites. As a consequence, the two satellite peaks at 2.68 and 2.87 eV appear much more prominent in Figure 4 than in Figure 5.

The spectral line shape observed upon deposition of the first monolayer of α-6T on Ag(111) (stage I) is very broad. A similar broadening or quenching of the molecular optical response has been observed for many other molecules in direct contact with a metal substrate[44−46] and has been attributed to the strong interaction and hybridization of the molecular and substrate electronic states. These states are localized at the interface and thus affect only the first organic monolayer. Indeed, upon deposition of the second layer, the DRS and DDRS spectra change significantly and distinct spectral features at about 2.5, 2.7, and 2.9 eV can be discerned. These can be attributed to excitonic states derived from the molecular highest occupied molecular orbital−lowest unoccupied molecular orbital transition.[47] It is not clear whether one of the higher-energy peaks at 2.7 and 2.9 eV, respectively, belongs to an independent excitonic transition, such as the upper Davydov component[31,48] of a split-up fundamental excitation or to the vibronic progression of a single electronic transition at 2.5 eV. In fact, the offset of the high-energy peaks is consistent with the findings of Garnier, who reported an energy quantum of 0.18 eV for the C═C stretch vibration in bulk α-6T.[49]

The situation is clearer for the spectra observed during growth stage III. Here the peaks are sharper such that the positions can be determined with better precision. From the green curves in Figure 5b we obtain initial peak positions at 2.32, 2.50, 2.68, and ∼2.87 eV, which are thus characteristic of the initial 3D nuclei of α-6T that form on top of the wetting layer. Upon subsequent growth into larger crystallites, the first two peaks shift toward 2.23 and 2.47 eV, respectively. Therefore, the spacing between the first two peaks is not constant but increases from 0.18 to 0.24 eV with increasing size of the α-6T crystallites. Consequently, these two peaks can only

DOI: 10.1021/acs.jpcc.5b08083
J. Phys. Chem. C 2015, 119, 24174−24181

be associated with two individual electronic states, such as two components of a Davydov split excitonic transition. On the other hand, the third peak (initially at 2.68 eV) appears to shift at the same rate as the second one. Besides the fact that the splitting of 0.18 eV coincides with the expected C=C vibration quantum, the constant offset of the third peak to the upper Davydov component (initially at 2.50 eV) suggests that it is a vibronic replica of the latter.

The absorption of single α-6T molecules in solution is peaked at 2.85 eV.[49] Instead, the fundamental transition found in the DRS and DDRS spectra for bilayer α-6T on Ag(111) at ∼2.5 eV is considerably red-shifted because of the interaction with the surrounding molecules and with the substrate. In the first layer, the α-6T molecules grow with their molecular planes parallel to the substrate.[8,50] This configuration increases the interaction between the adsorbed molecules and the substrate, leading to the aforementioned hybridization and a concomitant broadening of the optical signatures. The orientation of the molecules in the second layer is essentially the same as in the monolayer, but the spectral line shape is quite different because of the strongly reduced interaction with the substrate. As discussed in the previous section, the PEEM and DRS transients in Figure 2 suggest a restructuring of the first layer upon formation of the bilayer, involving a compression of the monolayer of up to ∼10%, consistent with ref 8. Such a compression could be achieved by slightly tilting the molecules around the long molecular axis.[51] In this case, the molecular axes would still be parallel to the surface, although the interaction of the substrate might be reduced. Nevertheless, the proximity to the surface will still lead to a strong coupling to the metal substrate such that the second layer can be considered the first "free" layer that can develop independent electronic states characteristic of a single sheet of molecules. In fact, the optical signature of the bilayer in Figures 4 and 5 resembles the line shape of the RDS spectra recorded for a single monolayer of α-6T on Cu(110)-(2 × 1)O.[28] In the latter case, the presence of the oxygen reduces the strong interaction of the α-6T layer with the copper substrate, whereas for α-6T on Ag(111) the first monolayer of α-6T could, indeed, play the role of an (optically inactive) buffer layer. Following the arguments in ref 28, it is then also conceivable that the absence of a sizable Davydov splitting at this growth stage is due to the fact that the molecules in the second layer in each crystalline domain form stacks with the same orientation and tilting direction. On the other hand, during growth stage III, the molecules will adopt a more bulk-like multilayer structure in which the molecules in subsequent layers are tilted in opposite directions, giving rise to the well-known herringbone stacking. As a result, the unit cell now contains at least two inequivalent molecules giving rise to a Davydov splitting, of the two peaks initially positioned at 2.50 and 2.68 eV. Again the DDRS spectra of the 3D crystallites in Figure 5 are quite similar to the RDS spectra obtained from the 3D islands grown on an α-6T wetting layer on Cu(110)-(2 × 1)O.[28] In either case the molecules will eventually adopt a structure that is close to that of bulk α-6T. It is therefore not surprising that the optical characteristics resemble those of the bulk, independent of the substrate or the intermediate structure of the wetting layer, as long as the latter is composed of flat-lying α-6T molecules. However, one should also keep in mind that the scattering geometry under which the optical response was measured are different in the two cases. Whereas in the RDS study of α-6T on Cu(110)-(2 × 1)O[28] the molecules were all uniaxially aligned along a single crystallographic direction and the angle of incidence was close to normal, in the present case, the molecules are aligned in three (rotationally equivalent) domains rotated by 120° with respect to each other and the angle of incidence in the DRS setup is about 65° off normal (see Figure 1). In fact, it can be shown for optically anisotropic media and for α-6T in particular[34] that the position and line shape of the spectral features may strongly depend on the relative orientation of the wavevector of the incident light and the transition dipole moment. This should be taken into account in a quantitative comparison of the data.

The size of the Davydov splitting is expected to be inversely proportional to the cube of the intermolecular distance.[48] Therefore, a shorter distance implies a stronger intermolecular interaction, such that the splitting between the Davydov components should increase. On the basis of their diffraction experiments, Yoshikawa and co-workers[8] suggested that the α-6T molecules would gradually approach each other with increasing film thickness. In fact, we observe a red shift of the two fundamental Davydov components initially at 2.32 and 2.50 eV. In agreement with Yoshikawa et al. there is also a slight increase of the spacing between the two Davydov components, consistent with a compression upon growth of the α-6T crystallites.

Finally, we observe a monotonous decrease of the DDRS signal during the final growth stage III. This is most likely due to the rapid increase of the height of the 3D crystallites, once the nucleation on the wetting layer has taken place. As already mentioned, only a small fraction (∼10%) of the surface area is actually covered by α-6T crystallites such that their average height reaches about 20 molecular layers (∼10 nm) toward the end of the growth experiment. Because α-6T is a strong absorber of light in the considered spectral range, the optical penetration depth is expected to be in the nanometer range only. As a consequence, the incremental changes of the reflectance should decay exponentially until, for thicknesses much larger than the penetration depth, the reflectance reaches a constant value and hence no incremental changes should be observed at all.

SUMMARY AND CONCLUSIONS

The combination of photoelectron emission microscopy (PEEM) and optical differential reflectance spectroscopy (DRS) is a versatile tool to study metal−organic interfaces. The ability for synchronous and real-time observation during growth was used to study the morphological and optical properties of organic thin films on a metal substrate, namely α-6T on Ag(111). On the basis of the correlation between the PEEM signal and the optical reflectance, we identify the stepwise evolution of the optical properties of the α-6T and its dependence on the thin film structure and morphology. We can divide the growth and the ensuing optical characteristics into three distinct stages.

(I) During the formation of the first monolayer, the electron yield monitored by PEEM increases homogeneously over the entire field of view, indicating that the molecules from small, homogeneously distributed 2D islands in equilibrium with a dilute 2D gas phase. The overall increase of the electron yield can be attributed to the formation of an interface dipole and the concomitant reduction of the work function. During this growth stage the differential reflectance spectra show only a weak and broad optical signature, due to the hybridization of the molecular and substrate electronic states as a consequence

DOI: 10.1021/acs.jpcc.5b08083
J. Phys. Chem. C 2015, 119, 24174−24181

of the strong interaction of the molecules with the metal substrate.

(II) During the growth of the second α-6T layer, a rearrangement of the molecules in the first monolayer (including a compression of up to 10%) takes place. The optical response of the α-6T bilayer differs markedly from that of the monolayer. The optical spectra reveal several peaks which are attributed to an excitonic state and its vibronic progression. The likely absence of a significant Davydov splitting suggests that the optical properties are dominated by the topmost molecular layer composed of translationally equivalent molecules, whereas the bottom layer can be considered as an optically inactive "buffer layer" to the metal substrate.

(III) The onset of 3D growth can be consistently determined from both the PEEM and the DRS data. While in PEEM the transition is marked by a sudden drop of the local electron yield and the concomitant appearance of dark spots in the images, the reflectance spectra exhibit a clear Davydov splitting characteristic of 3D crystallite growth. With increasing coverage, the optical signatures show a systematic shift as well as a continuous reduction of the incremental changes of the reflectance. The former is consistent with structural relaxations in the thicker films, whereas the latter is simply related to the increasing height of the 3D crystallites.

The analysis performed in this work can be extended to other metal−organic systems or heterostructures in order to obtain a comprehensive understanding of the electronic and optical properties of technologically relevant organic thin films.

■ ASSOCIATED CONTENT

Supporting Information

The Supporting Information is available free of charge on the ACS Publications website at DOI: 10.1021/acs.jpcc.5b08083.

Full image sequence of Figure 3 (AVI)

■ AUTHOR INFORMATION

Corresponding Authors

*E-mail: ebrahim.ghanbari@jku.at. Phone: +43 732 2468-5322. Fax: +43 732 2468-5315.
*E-mail: thorsten.wagner@jku.at.
*E-mail: peter.zeppenfeld@jku.at.

Notes

The authors declare no competing financial interest.

■ ACKNOWLEDGMENTS

This work was supported by the Austrian Science Fund FWF under project number P24528-N20. We thank Mike Ramsey from the University of Graz for the supply of the α-6T.

■ REFERENCES

(1) Forker, R.; Fritz, T. Optical Differential Reflectance Spectroscopy of Ultrathin Epitaxial Organic Films. *Phys. Chem. Chem. Phys.* **2009**, *11*, 2142−2155.

(2) Fahrenbach, A. C.; Warren, S. C.; Incorvati, J. T.; Avestro, A.-J.; Barnes, J. C.; Stoddart, J. F.; Grzybowski, B. A. Organic Switches for Surfaces and Devices. *Adv. Mater.* **2013**, *25*, 331−348.

(3) Forker, R.; Gruenewald, M.; Fritz, T. Optical Differential Reflectance Spectroscopy on Thin Molecular Films. *Annu. Rep. Prog. Chem., Sect. C: Phys. Chem.* **2012**, *108*, 34−68.

(4) Koller, G.; Berkebile, S.; Ivanco, J.; Netzer, F.; Ramsey, M. Device Relevant Organic Films and Interfaces: A Surface Science Approach. *Surf. Sci.* **2007**, *601*, 5683−5689.

(5) Horowitz, G.; Garnier, F.; Yassar, A.; Hajlaoui, R.; Kouki, F. Field-Effect Transistor Made With a Sexithiophene Single Crystal. *Adv. Mater.* **1996**, *8*, 52−54.

(6) White, M. S.; Kaltenbrunner, M.; Glowacki, E. D.; Gutnichenko, K.; Kettlgruber, G.; Graz, I.; Aazou, S.; Ulbricht, C.; Egbe, D. A. M.; Miron, M. C.; et al. Ultrathin, Highly Flexible and Stretchable PLEDs. *Nat. Photonics* **2013**, *7*, 811−816.

(7) Leising, G.; Tasch, S.; Meghdadi, F.; Athouel, L.; Froyer, G.; Scherf, U. Blue Electroluminescence With Ladder-Type Poly(Para-Phenylene) and Para-Hexaphenyl. *Synth. Met.* **1996**, *81*, 185−189.

(8) Yoshikawa, G.; Kiguchi, M.; Ikeda, S.; Saiki, K. Molecular Orientations and Adsorption Structures of α-Sexithienyl Thin Films Grown on Ag(110) and Ag(111) Surfaces. *Surf. Sci.* **2004**, *559*, 77−84.

(9) Kilian, L.; Umbach, E.; Sokolowski, M. Molecular Beam Epitaxy of Organic Films Investigated by High Resolution Low Energy Electron Diffraction (SPA-LEED): 3,4,9,10-Perylenetetracarboxylica-cid-Dianhydride (PTCDA) on Ag(111). *Surf. Sci.* **2004**, *573*, 359−378.

(10) Seidel, C.; Ellerbrake, R.; Gross, L.; Fuchs, H. Structural Transitions of Perylene and Coronene on Silver and Gold Surfaces: A Molecular-Beam Epitaxy LEED Study. *Phys. Rev. B: Condens. Matter Mater. Phys.* **2001**, *64*, 195418.

(11) Seidel, C.; Poppensieker, J.; Fuchs, H. Real-Time Monitoring of Phase Transitions of Vacuum Deposited Organic Films by Molecular Beam Deposition LEED. *Surf. Sci.* **1998**, *408*, 223−231.

(12) Wang, Y. L.; Ji, W.; Shi, D. X.; Du, S. X.; Seidel, C.; Ma, Y. G.; Gao, H.-J.; Chi, L. F.; Fuchs, H. Structural Evolution of Pentacene on a Ag(110) Surface. *Phys. Rev. B: Condens. Matter Mater. Phys.* **2004**, *69*, 075408.

(13) Moser, A.; Salzmann, I.; Oehzelt, M.; Neuhold, A.; Flesch, H.; Ivanco, J.; Pop, S.; Toader, T.; Zahn, D.; Smilgies, D.; et al. A Disordered Layered Phase in Thin Films of Sexithiophene. *Chem. Phys. Lett.* **2013**, *574*, 51−55.

(14) Ritley, K. A.; Krause, B.; Schreiber, F.; Dosch, H. A Portable Ultrahigh Vacuum Organic Molecular Beam Deposition System for In-Situ X-Ray Diffraction Measurements. *Rev. Sci. Instrum.* **2001**, *72*, 1453−1457.

(15) Gerlach, A.; Schreiber, F.; Sellner, S.; Dosch, H.; Vartanyants, I. A.; Cowie, B. C. C.; Lee, T.-L.; Zegenhagen, J. Adsorption-Induced Distortion of F_{16}CuPc on Cu(111) and Ag(111): An X-Ray Standing Wave Study. *Phys. Rev. B: Condens. Matter Mater. Phys.* **2005**, *71*, 205425.

(16) Gerlach, A.; Sellner, S.; Schreiber, F.; Koch, N.; Zegenhagen, J. Substrate-Dependent Bonding Distances of PTCDA: A Comparative X-Ray Standing-Wave Study on Cu(111) and Ag(111). *Phys. Rev. B: Condens. Matter Mater. Phys.* **2007**, *75*, 045401.

(17) Rager, A.; Gompf, B.; Düselen, L.; Mockert, H.; Schmeisser, D.; Göpel, W. Stability of Organic Thin Films on Inorganic Substrates: Prototype Studies Using Metal Phthalocyanines. *J. Mol. Electron.* **1989**, *5*, 227−238.

(18) Fukagawa, H.; Yamane, H.; Kera, S.; Okudaira, K. K.; Ueno, N. Experimental Estimation of the Electric Dipole Moment and Polarizability of Titanyl Phthalocyanine Using Ultraviolet Photo-electron Spectroscopy. *Phys. Rev. B: Condens. Matter Mater. Phys.* **2006**, *73*, 041302.

(19) Häming, M.; Greif, M.; Sauer, C.; Schöll, A.; Reinert, F. Electronic Structure of Ultrathin Heteromolecular Organic-Metal Interfaces: SnPc/PTCDA/Ag(111) and SnPc/Ag(111). *Phys. Rev. B: Condens. Matter Mater. Phys.* **2010**, *82*, 235432.

(20) Meyer zu Heringdorf, F.-J.; Reuter, M. C.; Tromp, R. M. Growth Dynamics of Pentacene Thin Films. *Nature* **2001**, *412*, 517−520.

(21) Wagner, T.; Fritz, D. R.; Zeppenfeld, P. Standing and Flat Lying α-6T Molecules Probed by Imaging Photoelectron Spectroscopy. *Org. Electron.* **2011**, *12*, 442−446.

(22) Fleming, A. J.; Netzer, F. P.; Ramsey, M. G. Nucleation and 3D Growth of Para -Sexiphenyl Nanostructures From an Oriented 2D Liquid Layer Investigated by Photoemission Electron Microscopy. *J. Phys.: Condens. Matter* **2009**, *21*, 445003.

DOI: 10.1021/acs.jpcc.5b08083
J. Phys. Chem. C 2015, 119, 24174−24181

(23) Fleming, A. J.; Berkebile, S.; Ules, T.; Ramsey, M. G. Pre-Nucleation Dynamics of Organic Molecule Self-Assembly Investigated by PEEM. *Phys. Chem. Chem. Phys.* **2011**, *13*, 4693−4708.
(24) Wagner, T.; Fritz, D. R.; Zeppenfeld, P. Probing Organic Nanostructures by Photoelectron-Emission Microscopy. *Appl. Surf. Sci.* **2013**, *267*, 26−29.
(25) Wagner, T.; Györök, M.; Huber, D.; Zeppenfeld, P.; Głowacki, E. D. Quinacridone on Ag(111): Hydrogen Bonding Versus Chirality. *J. Phys. Chem. C* **2014**, *118*, 10911−10920.
(26) Hosokai, T.; Gerlach, A.; Hinderhofer, A.; Frank, C.; Ligorio, G.; Heinemeyer, U.; Vorobiev, A.; Schreiber, F. Simultaneous In-Situ Measurements of X-Ray Reflectivity and Optical Spectroscopy during Organic Semiconductor Thin Film Growth. *Appl. Phys. Lett.* **2010**, *97*, 063301.
(27) Heinemeyer, U.; Broch, K.; Hinderhofer, A.; Kytka, M.; Scholz, R.; Gerlach, A.; Schreiber, F. Real-Time Changes in the Optical Spectrum of Organic Semiconducting Films and Their Thickness Regimes during Growth. *Phys. Rev. Lett.* **2010**, *104*, 257401.
(28) Sun, L.; Berkebile, S.; Weidlinger, G.; Denk, M.; Denk, R.; Hohage, M.; Koller, G.; Netzer, F. P.; Ramsey, M. G.; Zeppenfeld, P. Layer Resolved Evolution of The Optical Properties of α-Sexithiophene Thin Films. *Phys. Chem. Chem. Phys.* **2012**, *14*, 13651−13655.
(29) Toyoshima, H.; Inoue, K.; Hiraga, K.; Ohno, S.; Tanaka, M. Determination of Molecular Orientation of α-Sexithiophene on Passivated Si(001) by Means of Optical Reflectance Spectroscopic Methods. *Surf. Sci.* **2013**, *616*, 36−43.
(30) Kasha, M. Energy Transfer Mechanisms and the Molecular Exciton Model for Molecular Aggregates. *Radiat. Res.* **1963**, *20*, 55−70.
(31) Muccini, M.; Lunedei, E.; Taliani, C.; Beljonne, D.; Cornil, J.; Brédas, J. L. Interchain Interaction in a Prototypical Conjugated Oligomer from Polarized Absorption at 4.2 K: α-Sexithienyl Single Crystal. *J. Chem. Phys.* **1998**, *109*, 10513−10520.
(32) Muccini, M.; Schneider, M.; Taliani, C.; Sokolowski, M.; Umbach, E.; Beljonne, D.; Cornil, J.; Brédas, J. Effect of Wave-Function Delocalization on The Exciton Splitting in Organic Conjugated Materials. *Phys. Rev. B: Condens. Matter Mater. Phys.* **2000**, *62*, 6296−6300.
(33) Spano, F. C.; Silvestri, L.; Spearman, P.; Raimondo, L.; Tavazzi, S. Reclassifying Exciton-Phonon Coupling in Molecular Aggregates: Evidence of Strong Nonadiabatic Coupling in Oligothiophene Crystals. *J. Chem. Phys.* **2007**, *127*, 184703−184715.
(34) Weiser, G.; Möller, S. Directional Dispersion of The Optical Resonance of π-π* Transitions of α-Sexithiophene Single Crystals. *Phys. Rev. B: Condens. Matter Mater. Phys.* **2002**, *65*, 045203.
(35) Soukopp, A.; Glöckler, K.; Kraft, P.; Schmitt, S.; Sokolowski, M.; Umbach, E.; Mena-Osteritz, E.; Bäuerle, P.; Hädicke, E. Superstructure Formation of Large Organic Adsorbates on a Metal Surface: A Systematic Approach Using Oligothiophenes on Ag(111). *Phys. Rev. B: Condens. Matter Mater. Phys.* **1998**, *58*, 13882−13894.
(36) Wagner, T.; Fritz, D. R.; Zeppenfeld, P. α-6T on Ag(110): The Formation of The Wetting Layer. *Synth. Met.* **2011**, *161*, 2006−2010.
(37) Wagner, T.; Ghanbari, E.; Huber, D.; Zeppenfeld, P. The Growth of α-Sexithiophene Films on Ag(111) Studied by Means of PEEM With Linearly Polarized Light. *Ultramicroscopy* **2015**, DOI: 10.1016/j.ultramic.2015.06.013.
(38) Zaglmayr, H.; Hu, C. G.; Sun, L. D.; Zeppenfeld, P. Optical Referencing in Differential Reflectance Spectroscopy. *Meas. Sci. Technol.* **2014**, *25*, 115603.
(39) Grobosch, M.; Knupfer, M. Energy Level Alignment and Interface States at α-Sexithiophene/Ag Interfaces. *Org. Electron.* **2007**, *8*, 625−630.
(40) Ivanco, J.; Haber, T.; Resel, R.; Netzer, F.; Ramsey, M. Electronic and Geometric Structure of Electro-Optically Active Organic Films and Associated Interfaces. *Thin Solid Films* **2006**, *514*, 156−164.
(41) Kahn, A.; Koch, N. In *The Molecule-Metal Interface*; Wiley-VCH Verlag GmbH & Co. KGaA: Weinheim, Germany, 2013; pp 219−241.
(42) Chandekar, A.; Whitten, J. Ultraviolet Photoemission and Electron Loss Spectroscopy of Oligothiophene Films. *Synth. Met.* **2005**, *150*, 259−264.
(43) Ivanco, J.; Haber, T.; Krenn, J.; Netzer, F. P.; Resel, R.; Ramsey, M. Sexithiophene Films on Ordered and Disordered TiO_2(110) Surfaces: Electronic, Structural and Morphological Properties. *Surf. Sci.* **2007**, *601*, 178−187.
(44) Demuth, J. E.; Sanda, P. N. Observation of Charge-Transfer States for Pyridine Chemisorbed on Ag(111). *Phys. Rev. Lett.* **1981**, *47*, 57−60.
(45) Hu, Y.; Maschek, K.; Sun, L.; Hohage, M.; Zeppenfeld, P. Para-Sexiphenyl Thin Film Growth on Cu(110) and Cu(110)(2 × 1)O Surfaces. *Surf. Sci.* **2006**, *600*, 762−769.
(46) Flores, F.; Ortega, J. In *The Molecule-Metal Interface*; Wiley-VCH Verlag GmbH & Co. KGaA: Weinheim, Germany, 2013; pp 15−49.
(47) McIntire, M. J.; Manas, E. S.; Spano, F. C. Spontaneous Emission and Absorption in Model Aggregates of π-Conjugated Oligomers. *J. Chem. Phys.* **1997**, *107*, 8152−8164.
(48) Davydov, A. S. The Theroy of Molecular Excitons. *Phys.-Usp.* **1964**, *7*, 145.
(49) Garnier, F. Organic-Based Electronics a la Carte. *Acc. Chem. Res.* **1999**, *32*, 209−215.
(50) Zhang, H. L.; Chen, W.; Chen, L.; Huang, H.; Wang, X. S.; Yuhara, J.; Wee, A. T. S. C_{60} Molecular Chains on α-Sexithiophene Nanostripes. *Small* **2007**, *3*, 2015−2018.
(51) Oehzelt, M.; Berkebile, S.; Koller, G.; Ivanco, J.; Surnev, S.; Ramsey, M. α-Sexithiophene on Cu(110) and Cu(110)(2 × 1)O: An STM and NEXAFS Study. *Surf. Sci.* **2009**, *603*, 412−418.

DOI: 10.1021/acs.jpcc.5b08083
J. Phys. Chem. C 2015, 119, 24174−24181